Journal Name

ARTICLE TYPE

Cite this: DOI: 00.0000/xxxxxxxxxx

Electronic supplementary information for: Spontaneous Symmetry-breaking of Active Cluster Drives Directed Movement and Self-sustained Oscillation of Symmetric Rod-like Passive Particles

Ying Lan,[a] Man Xu,[a] Jinjiang Xie,[a] Yuehua Yang,[a] and Hongyuan Jiang*[a]

[a] *CAS Key Laboratory of Mechanical Behavior and Design of Materials, Hefei National Laboratory for physical Science at the Microscale, Department of Modern Mechanics, CAS Center for Excellence in Complex System Mechanics, University of Science and Technology of China, Hefei, Anhui 230026, China.*

Received Date
Accepted Date

DOI: 00.0000/xxxxxxxxxx

The Electronic Supplementary Information section contains additional figures and movies to show simulation details and theoretical predictions.

1 Simulation

1.1 The Numerical Model

In this work, we use a classical collision-based model [??] to investigate the directed movement and oscillation of symmetric rod-like passive particles (RPP) . We consider a rod-like passive particle confined by a harmonic potential in an active bath consisting of N_a spherical active particles with diameter σ_a. The length and width of the rod-like passive particle are L and σ_a, respectively. The position of each active particle is $\mathbf{r}_i$. The magnitude and orientation of active velocity of the i-th active particle are v_a and $\hat{\mathbf{u}}_i = (\cos\theta_i, \sin\theta_i)$, where θ_i is the angle between active velocity and x-axis. We assume the i-th active particle interacts with the j-th active particle via a pure repulsive Lennard-Jones (LJ) potential, $U_{ij} = k(\sigma_a/|\mathbf{r}_{ij}|)^{12}$ for $|\mathbf{r}_{ij}| < 2^{1/6}\sigma_a$, where k is the intensity of the interaction and $\mathbf{r}_{ij} = \mathbf{r}_j - \mathbf{r}_i$ is the relative position of the j-th active particle to the i-th active particle. And active particles interact with the rod-like passive particle via the similar LJ potential U_{ip}, where the j-th active particle is replaced by a virtual point at a distance $\sigma_a/2$ behind the boundary of the rod-like particle with $\mathbf{r}_{ip}$ perpendicular to the boundary in Fig. S1, and $\mathbf{r}_{ip}$ is the relative position of the virtual point to the i-th active particle.

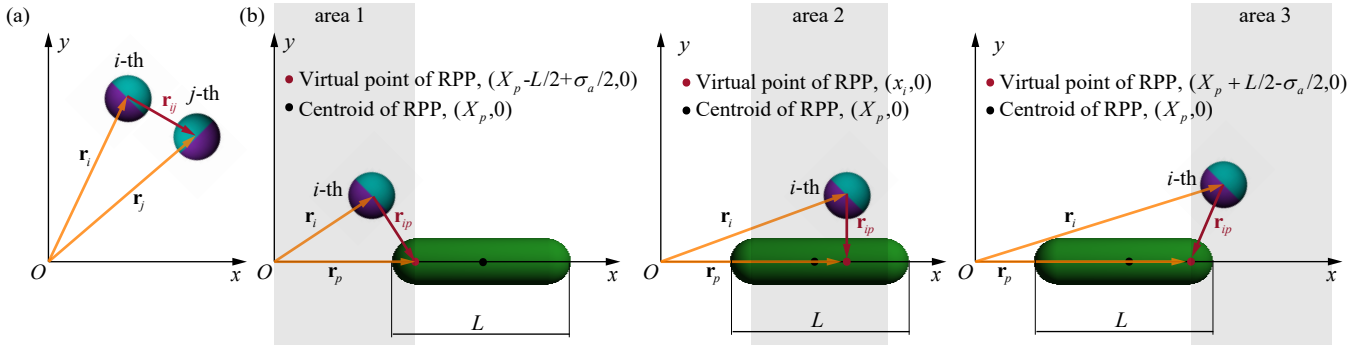

Fig. 1 Interaction between particles. (a) Interaction between two active particles. (b) Interaction between active particles and the passive particle when the i-th active particle locates in different areas (area 1-3) relative to the passive particle.

If we consider the low Reynolds number regime, the dynamics of the i-th active particle is given by overdamped Langevin equation [???]

$$\begin{aligned} \gamma_{Ta}\dot{\mathbf{r}}_i &= -\nabla_{\mathbf{r}_i}U_{ip} - \nabla_{\mathbf{r}_i}\sum_{j\neq i}U_{ij} + v_a\gamma_{Ta}\hat{\mathbf{u}}_i + \sqrt{2k_BT\gamma_{Ta}}\boldsymbol{\eta}_i^T, \\ \gamma_{Ra}\dot{\theta}_i &= \sqrt{2k_BT\gamma_{Ra}}\eta_i^R, \end{aligned} \tag{1}$$

where $\gamma_{Ta} = 3\pi\mu\sigma_a$ and $\gamma_{Ra} = \pi\mu{\sigma_a}^3$ are the translational and the rotational friction coefficient, and μ is the dynamic viscosity of water. k_BT is the thermal Boltzmann energy. η_i^T is the Gaussian white noise with zero mean and variance $\left\langle \eta_{i\alpha}^T(t)\eta_{j\beta}^T(t')\right\rangle = \delta_{ij}\delta_{\alpha\beta}\delta(t-t')$, where α and β denote Cartesian coordinates, and η_i^R is the Gaussian white noise with zero mean and variance $\left\langle \eta_i^R(t)\eta_j^R(t')\right\rangle = \delta_{ij}\delta(t-t')$.

For simplicity, we assume the rod-like passive particle can only move along x-axis and under the confinement of an external harmonic spring potential. Therefore, the motion of the rod-like passive particle [?????] can be given as

$$\gamma_p\dot{X}_p = -\sum_i \frac{\partial U_{ip}}{\partial X_p} - k_{eq}X_p, \tag{2}$$

where k_{eq} is harmonic potential stiffness, X_p and γ_p are the x-coordinate of RPP centroid and translational friction coefficient of RPP along x-axis.

1.2 The Simulation Procedure

The parameters used in the simulation are listed in Table **??**. We choose σ_a, $\tau = 1/D_R$ and k_bT as the unit of length, time and energy to normalize all the equations, where $D_R = k_BT/\gamma_{Ra}$ is the rotational diffusivity of active particles. Unless otherwise specified, all variables in the following sections will be expressed in dimensionless form. Our model consists of N_a spherical active particles and one rod-like passive particle. Furthermore, periodic boundary conditions is used and the simulation box is a rectangle ($L_x \times L_y$). The area fraction of active particles is defined as $\phi = N_aS_a/(L_xL_y - S_p)$, where

Table 1 Summary of the parameters used in the model calculations.

Parameter	Description	Value from experiments	Value in simulation	Value in theory
σ_a	Diameter of active particle, μm	$1 \sim 3$ [??]	2	-
v_a	Self-propelled speed, $\mu m \cdot s^{-1}$	19.3 [?]	19.3	19.3
γ_{Ta}	Active translational friction coefficient, $kg \cdot s^{-1}$	10^{-8} [?]	1.6×10^{-8}	-
γ_{Ra}	Active rotational friction coefficient, $kg \cdot m^2 s^{-1}$	10^{-20} [??]	2.1×10^{-20}	-
τ	Persistent time of diffusion, s	-	5.2	-
T	Temperature of the system, K	$295 \sim 300$ [??]	300	-
μ	Dynamic viscosity of water, $kg \cdot m^{-1}s^{-1}$	10^{-3} [??]	0.9×10^{-3}	-
L	Length of passive particle, μm	131 [?]	100	100
γ_p	Passive translational friction coefficient, $kg \cdot s^{-1}$	-	5.4×10^{-8}	5.4×10^{-8}

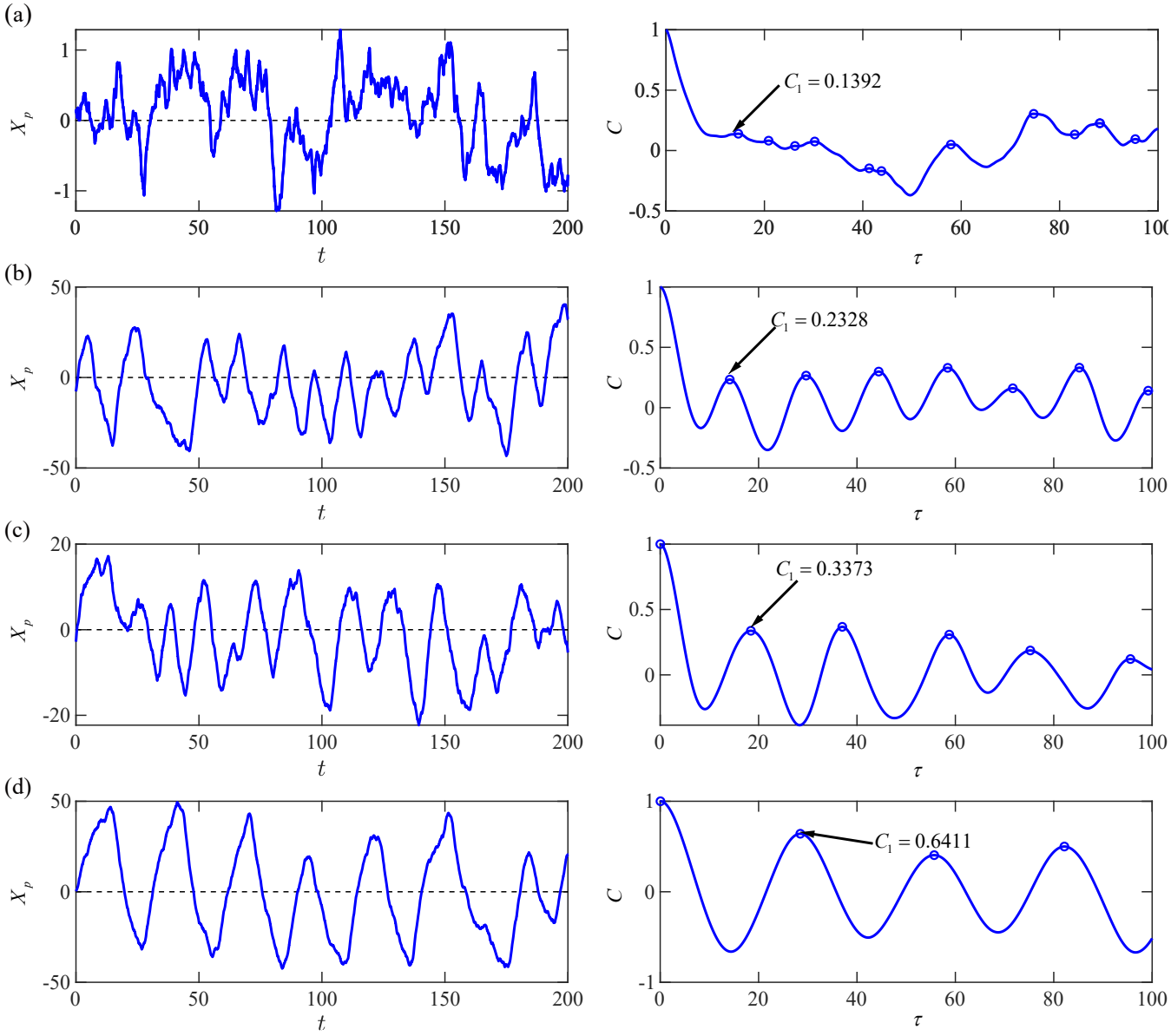

Fig. 2 The position of passive particle X_p and the autocorrelation function $C(\tau)$ of X_p. (a) $L = 5$, $v_a = 5$, (b) $L = 25$, $v_a = 50$, (c) $L = 40$, $v_a = 30$, and (d) $L = 50$, $v_a = 40$.

$S_a = \pi\sigma_a^2/4$ and $S_p = L\sigma_a - (1-\pi/4)\sigma_a^2$ are the projected areas of an active particle and the rod-like passive particle, respectively. Based on previous work[?], we choose $\phi = 0.2$ to enable active particles to cluster around the long rod-like passive particle and fail to cluster in the absence of the passive particle.

We use the modified LAMMPS to execute the simulation. The translational friction coefficient of the rod-like passive particle is calculated by software package HYDRO++[?]. The initial distribution of active particles is a rectangular lattice with random $\hat{\mathbf{u}}_i$[?]. To ensure that the results are independent of the initial condition and dynamically stabilized, the system is relaxed for 80 τ before sampling.

The size of the simulation area is selected according to the following conditions: (1) $L_x/L_{cx} \geq 5$, $L_y/L_{cy} \geq 5$, where L_{cx} and L_{cy} are the average length and width of the areas consisting of active particles clustering around the rod-like passive particle; (2) $N_c/N_a \leq 0.1$, where N_c is the number of neighbor particles. The first condition can reduce the influence of periodic boundary conditions on simulation results. The second condition ensures that the density of active particles outside the cluster is nearly unperturbed when active particles cluster around the rod-like particle. As a result, we choose $L_x = 300$ and $L_y = 200$ in our simulations.

1.3 Details of Periodic Movement

1.3.1 Judging Criteria of Periodic Motion

Whether the movement of the passive particle is a periodic oscillation can be identified by the autocorrelation function $C(\tau)$ of its displacement of passive particle X_p[?]. The autocorrelation function $C(\tau)$ is defined as $\langle X_p(t)X_p(t+\tau)\rangle / \langle X_p(t)X_p(t)\rangle$, where $\langle\cdot\rangle$ means the time average. We use the first positive peak value C_1 of the autocorrelation function to determine whether the movement of the passive particle is periodic. Generally, C_1 ranges from 0 to 1, and the larger the value of C_1 is, the closer the movement is to periodic oscillation. Due to the active noise, C_1 can't reach 1. In our simulation, we

choose the threshold of periodic motion as $C_t = 0.3$. When $C_1 < C_t$, the movement of the passive particle is dominated by random motion and not a periodic oscillation (Fig. S2a-b). When $C_1 \geq C_t$, the passive particle undergoes periodic oscillation (Fig. S2c-d).

1.3.2 Period and Amplitude of Self-sustained Oscillation of Passive Particle

The oscillation period of the passive particle is quantified as the average interval between the adjacent maximum of the autocorrelation function of X_p. The oscillation amplitude of the passive particle is calculated as one half of the average difference between adjacent maximums and minimums of X_p.

1.4 Spontaneous Symmetry Breaking of Neighboring Active Particles

In the main text, we demonstrate the spontaneous symmetry breaking of neighboring active particle distribution around the free passive particle leads to the emergence of cluster polarity and asymmetric resultant force from active particles that drives the directed motion of the passive particle. Furthermore, we also find the persistence time of the cluster polarity or directed motion of passive particle increases with N_c. What's more, the motility of the rod (speed and persistence) increases with the rod length (L), as shown in Fig. S3(a)-(b).

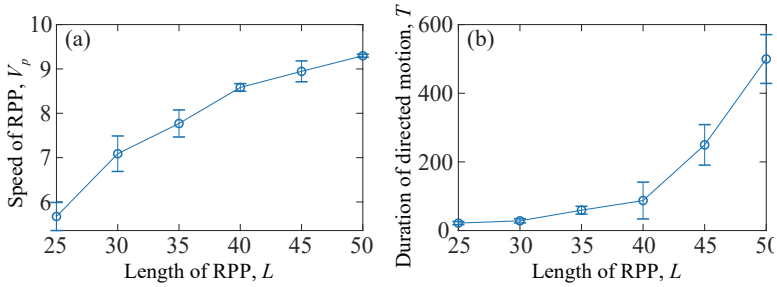

Fig. 3 The net motion of RPP. It indicates a net forward motion (a) and backward motion (b) of RPP ($v_a = 80$).

As demonstrated in Fig. 2(e) of our main text, the polarity and size of the active clusters are fluctuating. Furthermore, higher velocity or larger RPP can suppress the stochasticity of active noise. As shown in Fig. S4, the rod-like passive particle can have a net forward and backward motion, respectively, which lasts for 16000 and is larger than the sampling time in our manuscript (Fig. S4(a) insert). It can be observed that the result of a net motion appears in a specific simulated sample. The probability of being forward and backward in different samples is equal. So, the motion of the rod remains a net motion instead of a zero average net effect.

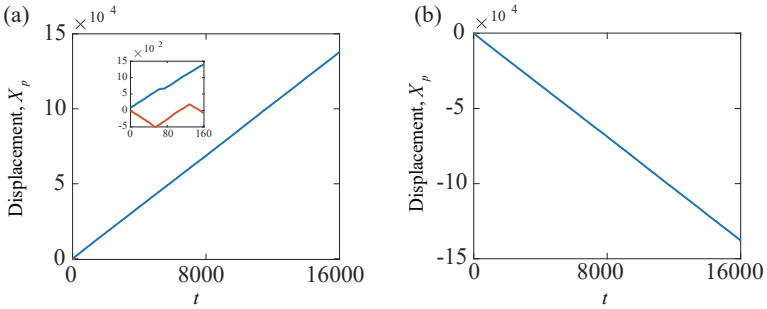

Fig. 4 The net motion of RPP. It indicates a net forward motion (a) and backward motion (b) of RPP ($v_a = 80$).

The above results are similar for self-sustained periodic oscillation when k_{eq} is finite. Fig. S5a shows probability distribution of $(n^- - n^+)/(n^- + n^+)$, where n^+ and n^- are the number of active particles moving along the positive and negative directions of x-axis relative to passive particle at a certain time. Apparently, the spontaneous symmetry breaking of neighboring active particle distribution still exists for the self-sustained periodic oscillation of passive particle (Fig. S5a). Furthermore, we also find the persistence time of the cluster polarity or directed motion of passive particle increases with N_c when k_{eq} is finite (Fig. S5b).

1.5 Negative Viscosity and Force Thickening Effect

When the passive particle is towed with a constant force F_d (or a constant velocity V_p), the effective viscosity can be defined as $\gamma_e = F_d/V_p$. Thus, the opposite signs of F_d and V_p indicate the effective viscosity of the active bath is negative. Specifically, the negative slope region ($dF_d/dV_p < 0$) of F_d-V_p curve is unstable since the passive particle moves faster under bigger resistance force in this regime (Fig. 5d in our main text), which is similar to the instability of negative stiffness during spontaneous oscillation of hair bundles in internal ears[?] . Our results are similar to the "negative" viscosity in the active microrheology[?] , where one measures the mobility[???] or the effective friction[?] of the tracer particle driven by a constant force or a constant velocity. It should be noted that the local "negative" viscosity in active microrheology is not equivalent to global "negative" viscosity in bulk rheology. In bulk rheology, "negative" effective shear viscosity means that a shear stress must be applied in a direction opposing the flow to maintain a fixed shear rate[??] .

What's more, in our previous work[?] ,we observed that the chevrons maintain a directed motion along their main axis. As active particles accumulate around the sharp corners of the chevrons, the chevrons spontaneously maintain a constant velocity without any external pulling force, which suggests the presence of a negative viscosity.

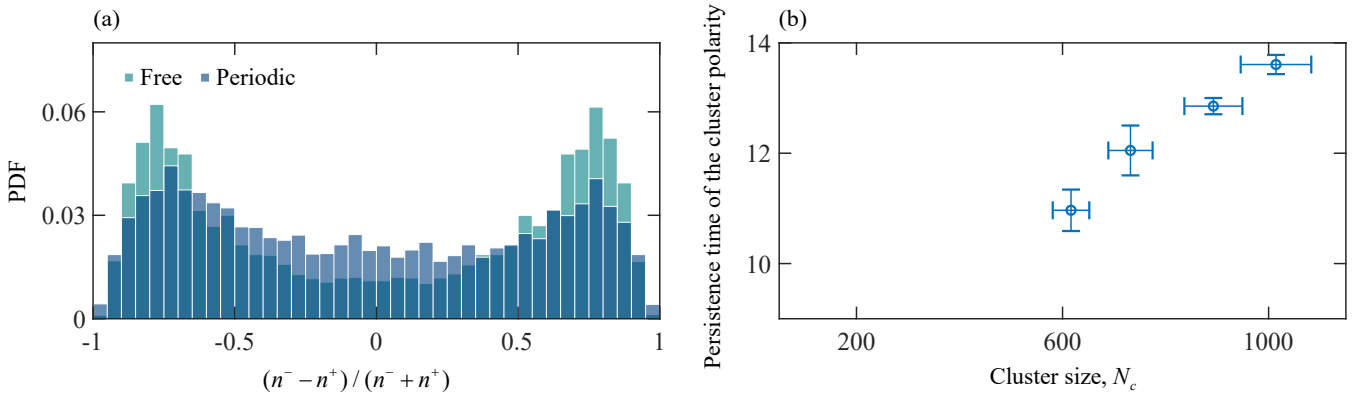

Fig. 5 Spontaneous symmetry breaking of neighboring active particle drives the self-sustained oscillation of passive particle. (a) Probability distribution of $(n^- - n^+)/(n^- + n^+)$, where n^+ and n^- are the number of active particles moving along the positive and negative directions of x-axis relatively to passive particle at a certain time. (b) Persistence time of directed motion increases with cluster size.

The results in Fig.5 and Fig.6 in our main text depend on the negative viscosity. Fig. S6 shows negative viscosity arises with higher active velocity and larger length of the passive particle. What's more, the self-sustained oscillation and forced oscillation of RPP similar to our manuscript would appear due to negative viscosity effect. The phase diagram of Fig. S6 is consistent with Fig. 3(a) in our main text.

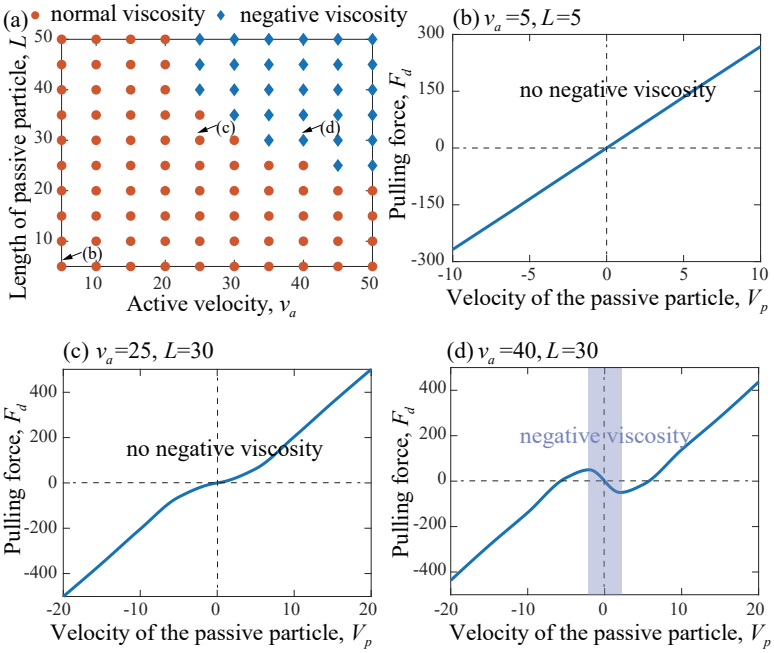

Fig. 6 Negative viscosity phase diagram. (a) shows negative viscosity phase diagram for different passive particle lengths or active velocities. (b)-(d) show three different cases for the curve , which marked with arrows in (a). (b) and (c) show no negative viscosity effect. (d) shows the negative viscosity effect appears.

Furthermore, we find that the effective viscosity γ_e of the active bath nonlinearly depends on F_d (Fig. S7), which shows the force thickening effect. This thickening behaviour correlates with the development of the active cluster surrounding the passive particle, in which active particles accumulate behind the passive particle and deplete in front of it (inserts in Fig. 5a). Strong external force delocalizes the neighboring particle from active cluster, resulting in a pronounnced force-thickening behavior of the single-particle friction. The similar force thickening effect has been predicted by simulations and observed experimentally[???].

1.6 A rotatable RPP

Our results are still applicable if the rod-like passive particle (RPP) is able to rotate. To confirm this conclusion, we performed some new calculations. Fig. S8(a)-(c) shows active particles still cluster around the rotatable RPP. The tail detachment of a group of particles from the cluster is also observed in Fig. S8(b). We can construct a body frame with the major axis of the RPP as the x-axis. In this body frame, the RPP shows a long-time directed motion along the x-axis and a stochastic motion along the y-axis, as seen in Fig. S8(d). Fig. S8(e) also shows that the number of neighboring particles (the cluster size) is highly dynamic. Comparing (d) with (f), we find that the rotational degree of freedom suppresses the RPP's directed motion, which randomizes the direction of the RPP's motion.

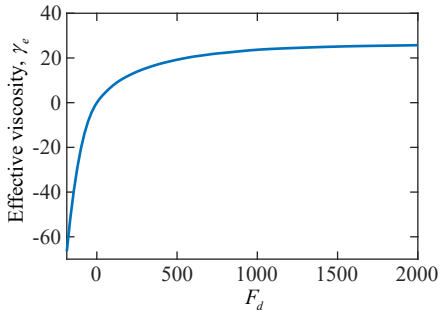

Fig. 7 The relationship between effective viscosity γ_e and F_d shows force thickening effect.

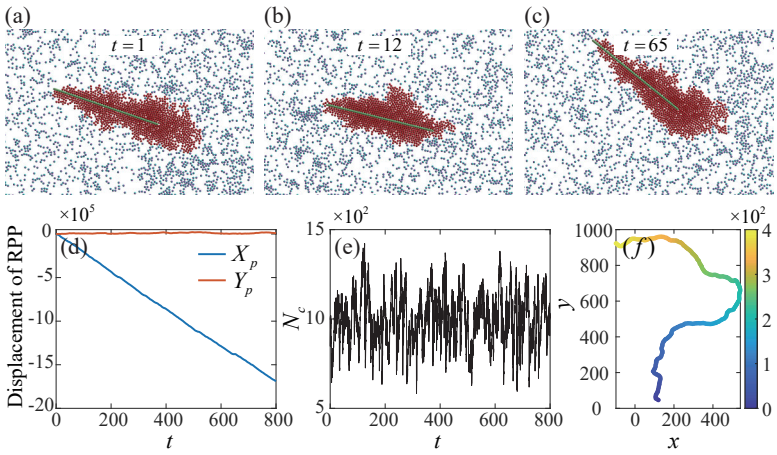

Fig. 8 Active cluster around a rotatable RPP. (a)-(c) show the distribution of active cluster around a rotatable RPP (L=50). (d) Evolution of RPP's displacement. (e) Trajectory of RPP.

1.7 The system reaching the threshold for MIPS

Moreover, when exploring the system reaching the threshold for MIPS, the active system without passive particles is divided into low density region and high density region, as shown in Fig. S9(a) and (b). When a rod-like passive particle is immersed in active systems, the case is slightly different. The phase separation process is accelerated and the cluster in the system is larger than the one in the system without a passive particle, as shown in Fig. S9(c). This indicates that the rod-like passive particle is in favor of nucleation. However, the rod-like passive particle is removed from the large active cluster and has no ability to go through the large cluster.

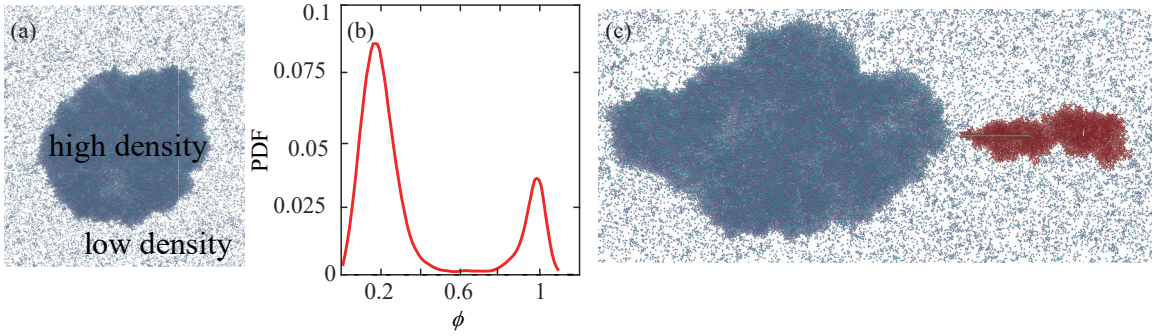

Fig. 9 The active cluster with the active system reaches the threshold for MIPS. (a) the low density and high density phases in the active system without passive particles. (b) Probability distribution of the area fraction. (c) Snapshots of the active system with a RPP. The active particle marked in red is neighboring particle.

2 Theoretical Model

2.1 Minimal 1D Theoretical Model

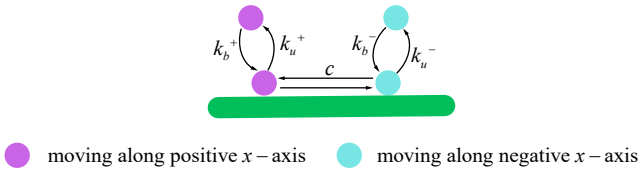

Fig. 10 Sketch of 1D theoretical model. There are N active particles in the system. The active particles can switch direction and attach to or detach from the passive particle randomly. Among active particles attaching to passive particle, there are n^+ and n^- active particles moving along the positive and negative directions of x-axis with the velocity of v^+ and v^-, respectively. c is the mutual conversion rate between the two populations of active particles. k_b^+ and k_u^+ (k_b^- and k_u^-) are the binding rates of free active particles and the unbinding rates of attached active particles moving along the positive (negative) directions of x-axis, respectively.

In this paper, we proposed a simple 1D theoretical model to verify our mechanism. Our model consists of a rod-like passive particle with length L (marked with green in Fig. S10), and N active particles. For simplicity, we assume that the active particles can only move along x-axis with constant speed v_a, and they can switch direction and attach to or detach from the passive particle randomly. Among active particles attaching to the passive particle, there are n^+ and n^- active particles moving along the positive and negative directions of x-axis with the velocity of v^+ and v^-, respectively. Furthermore, we also choose σ_a, $\tau = 1/D_R$ and k_BT as the unit of length, time and energy to normalize all equations in our theoretical model. When not specified, physical quantities will be expressed in dimensionless form.

The force on the passive particle applied by an active particle moving along the positive and negative direction of x-axis, i.e., F^+ and F^-, are

$$\begin{aligned} F^+ &= \gamma_{ap}(v^+ - \dot{X}_p), \\ F^- &= \gamma_{ap}(v^- - \dot{X}_p), \end{aligned} \tag{3}$$

where γ_{ap} is the friction coefficient between passive particle and active particles, and X_p and $\dot{X}_p = V_p$ are the position and velocity of centroid of passive particle, respectively. The force balance equation of the active particles are

$$\begin{aligned} \gamma_a v^+ &= -F^+ + \gamma_a v_a, \\ \gamma_a v^- &= -F^- - \gamma_a v_a. \end{aligned} \tag{4}$$

Therefore, the force balance equation of the passive particle is

$$n^+F^+ + n^-F^- - \gamma_p \dot{X}_p - k_{eq}X_p = 0, \tag{5}$$

where k_{eq} is the stiffness of harmonic potential, and γ_p is the viscous drag coefficient of passive particle.

The active particles can switch direction and attach to or detach from the passive particle randomly in our theory. So, the time evolution of two populations of active particles moving along the positive and negative directions of x-axis with the velocity of v^+ and v^- can be described by

$$\begin{aligned} \dot{n}^+ &= cn^- - cn^+ + k_b^+(N - n^+ - n^-) - k_u^+ n^+, \\ \dot{n}^- &= cn^+ - cn^- + k_b^-(N - n^+ - n^-) - k_u^- n^-, \end{aligned} \tag{6}$$

where N is the total number of active particles in the system, c is the mutual conversion rate between the two populations of active particles. k_b^+ and k_b^- are the binding rates of free active particles moving along the positive (negative) directions of x-axis, respectively. k_u^+ and k_u^- are the unbinding rates of attaching active particles moving along the positive (negative) directions of x-axis, respectively. The binding rate of active particles decreases exponentially with the relative velocity of active particle to the passive particle, i.e, $k_b^+ = k_{b0}^+ e^{-A\left(v_a - \dot{X}_p\right)^2/v_a^2}$, and $k_b^- = k_{b0}^- e^{-A\left(-v_a - \dot{X}_p\right)^2/v_a^2}$, where A is a positive constant, k_{b0}^+ and k_{b0}^- are the binding rate constants. Conversely, the unbinding rate of attached active particles increases exponentially with the relative velocity of active particle to the passive particle, i.e, $k_u^+ = k_{u0}^+ e^{B\left(v^+ - \dot{X}_p\right)^2/v_a^2}$ and $k_u^- = k_{u0}^- e^{B\left(v^- - \dot{X}_p\right)^2/v_a^2}$, where B is a positive constant, and k_{u0}^+ and k_{u0}^- are the unbinding rate constants.

To compare the results of our theoretical model and simulations, the same dimensionless parameters are used as shown in Table **??**. The values of other free parameters in our theory are $N = 2000, \gamma_{ap} = 0.05$, $k_{b0}^+ = k_{b0}^- = 0.003$, $k_{u0}^+ = k_{u0}^- = 0.09$, $c = 0.3$, $A = 1 \times 10^{-6}$, and $B = 1.5625$, unless otherwise specified.

Table 2 Dimensionless parameters used in the simulations and theoretical model.

Parameter	Description	Value in simulation	Value in theory
v_a	Self-propelled speed	50	50
γ_{Ta}	Active translational friction coefficient	3	3
γ_p	Passive translational friction coefficient	25	25
k_{eq}	the stiffness of harmonic potential	$0, 4$, and ∞	$0, 4$, and ∞
L	Length of passive particle	50	50

2.2 Theoretical Results

2.2.1 Dynamics of the Rod-Like Passive Particle under Different Strength of Harmonic Potential

In Fig. S11, we show that the passive particle can keep a long-live directed motion or a periodic oscillation by tuning the strength of harmonic potential, which is consistent with our simulation. If k_{eq} goes to infinity, the position of the rod-like passive particle is fixed and $n^+ = n^-$ at the stable state (Fig. S11a). When $k_{eq} = 0$, the free passive particle moves either forward (Fig. S11b) or backward (Fig. S11c) at a constant speed depending on the initial values of n^+ and n^-. Notably, the constant speed is nearly the same as the free speed of the passive particle in our simulation when we use the same parameters. It should be noted that due to the lack of stochastic thermal noise in our simplified theory, the free passive particle can't switch direction. If k_{eq} is finite, we find the rod-like passive particle can undergo self-sustained periodic oscillation (Fig. S11d). In this 1D theoretical model, we can define the polarity and size of active cluster as $P_x = n^- - n^+$ and $N_c = n^- + n^+$, respectively.

2.2.2 Self-sustained Periodic Oscillation of Passive Particle

In our simplified theory, we can also investigate how the velocity of active particles v_a and the length of passive particle L determine the movement of passive particle (Fig. S12a) and the size of active cluster (Fig. S12b), and how external constraint k_{eq} and viscous drag γ_p affect the period (Fig. S12c) and amplitude (Fig. S12d) of oscillation. As shown in Fig. S12, the results of our theoretical model agree with the simulation well.

2.2.3 Relationship between V_p and F_d

When a rod-like passive particle ($k_{eq} = 0$) is towed along the x-axis at a constant velocity V_p, we have $\dot{X}_p = V_p$ and Eq. (5) should be modified to

$$n^+F^+ + n^-F^- - \gamma_p \dot{X}_p + F_d = 0. \tag{7}$$

When the system reaches a steady state, Eq. (6) becomes

$$\begin{aligned} 0 &= cn^- - cn^+ + k_b^+(N - n^+ - n^-) - k_u^+ n^+, \\ 0 &= cn^+ - cn^- + k_b^-(N - n^+ - n^-) - k_u^- n^-. \end{aligned} \tag{8}$$

By solving Eq. (7) and (8), we obtain

$$\begin{aligned} n^+ &= \frac{N(ck_b^+ + ck_b^- + k_b^+k_u^-)}{2ck_b^+ + 2ck_b^- + ck_u^+ + ck_u^- + k_b^-k_u^+ + k_b^+k_u^- + k_u^+k_u^-}, \\ n^- &= \frac{N(ck_b^+ + ck_b^- + k_b^-k_u^+)}{2ck_b^+ + 2ck_b^- + ck_u^+ + ck_u^- + k_b^-k_u^+ + k_b^+k_u^- + k_u^+k_u^-}, \\ F_d &= \frac{\gamma_{ap}\gamma_a N[(2ck_b^+ + 2ck_b^- + k_b^+k_u^- + k_b^-k_u^+)V_p - (k_b^+k_u^- - k_b^-k_u^+)v_a]}{(\gamma_{ap} + \gamma_a)(2ck_b^+ + 2ck_b^- + ck_u^+ + ck_u^- + k_b^-k_u^+ + k_b^+k_u^- + k_u^+k_u^-)} + \gamma_p V_p. \end{aligned} \tag{9}$$

As a result, we obtain the cluster N_c and the polarity P_x of attaching active particles as the function of V_p. As shown in Fig. 5b of the main text, the F_d-V_p relationship obtained from our simplified 1D theoretical model agree with the simulation results very well.

In this simplified 1D theoretical model, the rod-like passive particle can also be towed with a constant force F_d along the x-axis. The main results are similar to those of the constant velocity case. Consistent with our simulations, when the pulling force is located in [-$F_{d,c}$,$F_{d,c}$], the passive particle velocity is bistable and then able to snap through between bistable states.

2.2.4 Two Different Oscillations Triggered by the Passive Particle's Velocity Jumping-off

By using this simplified 1D model, we can also reproduce the two different oscillations of the passive particle observed in our simulations (Fig. 6 in the main text). We find the oscillatory trajectories of F_d-V_p curve in the above two cases are quite different. For periodic linear force loading, the system follows a limit cycle (marked with the blue lines), whose trajectory mainly emerges in the stable straight segment of the F_d-V_p curve (Fig. S13a). In contrast, the limit cycle of the self-sustained oscillation does not coincide with the F_d-V_p curve (Fig. S13b) since the force provided by the spring is not constant.

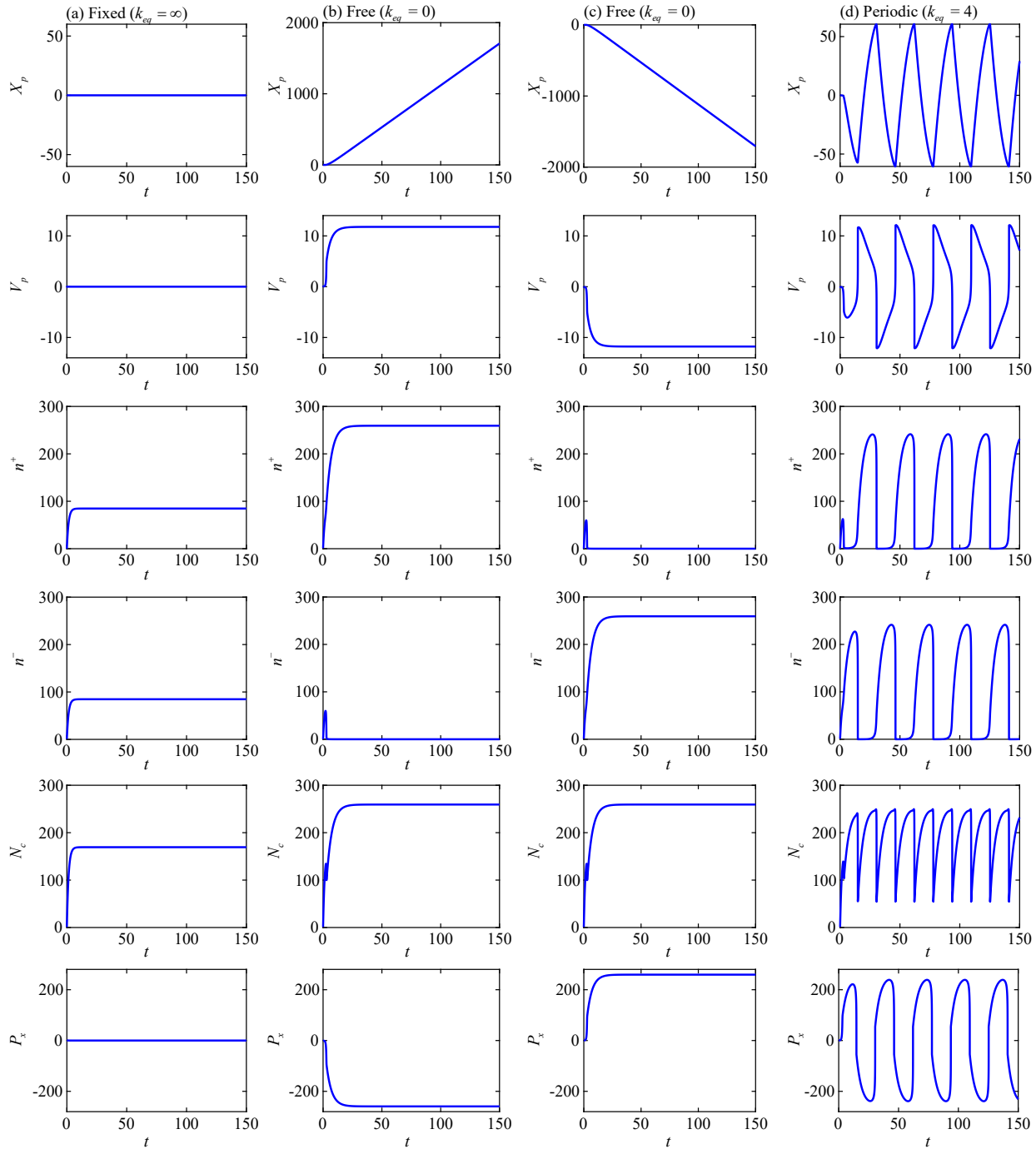

Fig. 11 Dynamics of the Rod-Like Passive Particle under Different Strength of Harmonic Potential. (a) When $k_{eq} = \infty$, the passive particle is fixed. (b) When $k_{eq} = 0$, the free passive particle moves forward at a constant speed with initial condition $n_0{}^+ > n_0{}^-$. (c) As $k_{eq} = 0$, the free passive particle moves backward at a constant speed with initial condition $n_0{}^+ < n_0{}^-$. (d) When $k_{eq} = 4$, the rod-like passive particle can undergo self-sustained periodic oscillation.

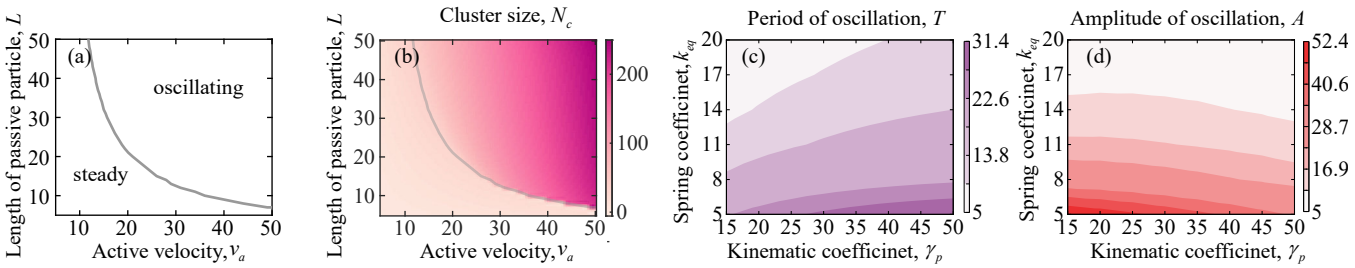

Fig. 12 Self-sustained periodic oscillation of passive particle predicted in our theoretical model. (a) Phase diagram of the passive particle movement and (b) cluster size. The period (c) and amplitude (d) of the periodic oscillation depends on γ_p and k_{eq}. Here, we assume $k_{b0}^{+} = k_{b0}^{-} = 0.0006 v_a$ and $k_{u0}^{+} = k_{u0}^{-} = 4.5/L$.

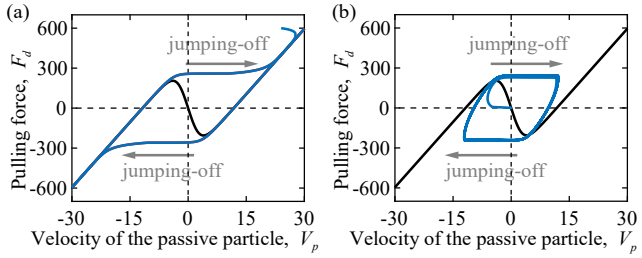

Fig. 13 Two different oscillations triggered by the velocity jumping-off. (a) The oscillatory trajectories of F_d-V_p curve for periodic linear force loading. (b) The oscillatory trajectories of F_d-V_p curve for the self-sustained oscillation. The black curves are the F_d-V_p curves as the passive particle is towed along the x-axis at a constant velocity V_p. The blue curves are the corresponding oscillations trajectories.

3 Captions of Supplementary Movies.

Supplementary movie 1. Four typical cases of passive particle movement and active cluster structure. (a) Fixed passive particle with $k_{eq} = \infty$ and $v_a = 50$. (b) Free passive particle with $k_{eq} = 0$ and $v_a = 50$. (c) Partially free passive particle undergoing periodic oscillation with $k_{eq} = 4$ and $v_a = 50$. (d) Partially free passive particle undergoing stochastic movement with $k_{eq} = 4$ and $v_a = 15$.

Supplementary movie 2. Aggregation states of neighboring particles around the passive particle with different active velocities (v_a) and the length of the passive particle (L). (a) No aggregation for $v_a = 5$ and $L = 5$. (b) No aggregation for $v_a = 50$ and $L = 5$. (c) No aggregation for $v_a = 5$ and $L = 50$. (d) Aggregation of active particles for $v_a = 50$ and $L = 50$.

Supplementary movie 3. The appearance and disappearance of "spontaneous broken symmetry of active cluster" by controlling the velocity of the passive particle. (a) The structure and dynamics of active cluster. (b) Time evolution of the position of the passive particle, the polarity of the cluster, and the cluster size.

Supplementary movie 4. The detailed process of active cluster detachment in Fig. 4g. (a) The structure and dynamics of active cluster. (b) Cluster size (N_c). (c) Cluster polarity (P_x).

Supplementary movie 5. The velocity jumping-off during the forced oscillation of passive particle. (a) The periodic linear force applied on the passive particle (F_d). (b) The relationship between the velocity of passive particle (V_p) and the external force (F_d). (c) The velocity of passive particle (V_p) and the polarity of an active cluster (P_x). (d) The structure and dynamics of active cluster.

Supplementary movie 6. The velocity jumping-off during the self-sustained periodic oscillation of passive particle. (a) The external force from the harmonic potential (F_d). (b) The relationship between the velocity of passive particle (V_p) and the external force (F_d). (c) The velocity of passive particle (V_p) and the polarity of the active cluster (P_x). (d) The structure and dynamics of active cluster.

Notes and references

L. Angelani, R. Di Leonardo and G. Ruocco, *Physical Review Letters*, 2009, **102**, 048104.

L. Angelani and R. Di Leonardo, *New Journal of Physics*, 2010, **12**, 113017.

L. Angelani, C. Maggi, M. Bernardini, A. Rizzo and R. Di Leonardo, *Physical Review Letters*, 2011, **107**, 138302.

L. Angelani and R. Di Leonardo, *Computer Physics Communications*, 2011, **182**, 1970–1973.

F. Turci and N. B. Wilding, *Physical Review Letters*, 2021, **127**, 238002.

A. Kaiser, H. Wensink and H. Löwen, *Physical Review Letters*, 2012, **108**, 268307.

A. Kaiser, K. Popowa, H. Wensink and H. Löwen, *Physical Review E*, 2013, **88**, 022311.

A. Kaiser, A. Peshkov, A. Sokolov, B. Ten Hagen, H. Löwen and I. S. Aranson, *Physical Review Letters*, 2014, **112**, 158101.

C. Wang and H. Jiang, *Soft Matter*, 2020, **16**, 4422–4430.

G. Mino, T. E. Mallouk, T. Darnige, M. Hoyos, J. Dauchet, J. Dunstan, R. Soto, Y. Wang, A. Rousselet and E. Clement, *Physical Review Letters*, 2011, **106**, 048102.

J. Tong, D. Wang, Y. Liu, X. Lou, J. Jiang, B. Dong, R. Dong and M. Yang, *Proceedings of the National Academy of Sciences*, 2021, **118**.

H. C. Berg, *E. coli in Motion*, Springer Science & Business Media, 2008.

J. Bialké, T. Speck and H. Löwen, *Physical Review Letters*, 2012, **108**, 168301.

P. Nelson, *Biological physics*, WH Freeman New York, 2004.

C. Bechinger, R. Di Leonardo, H. Löwen, C. Reichhardt, G. Volpe and G. Volpe, *Reviews of Modern Physics*, 2016, **88**, 045006.

P. Liu, H. Zhu, Y. Zeng, G. Du, L. Ning, D. Wang, K. Chen, Y. Lu, N. Zheng, F. Ye *et al.*, *Proceedings of the National Academy of Sciences*, 2020, **117**, 11901–11907.

L. Le Goff, D. Bozovic and A. Hudspeth, *Proceedings of the National Academy of Sciences*, 2005, **102**, 16996–17001.

G. Foffano, J. Lintuvuori, K. Stratford, M. Cates and D. Marenduzzo, *Physical Review Letters*, 2012, **109**, 028103.

M. Knežević, L. E. Avilés Podgurski and H. Stark, *Scientific Reports*, 2021, **11**, 1–10.

C. R Reichhardt and C. Reichhardt, *Physical Review E*, 2015, **91**, 032313.

L. G Wilson and C. K Poon, *Physical Chemistry Chemical Physics*, 2011, **13**, 10617–10630.

F. A. G. Daza, A. M. Puertas, A. Cuetos and A. Patti, *Journal of Colloid and Interface Science*, 2022, **605**, 182–192.

F. Kobayashi, Y. Sasaki, S. Fujii, H. Orihara and T. Nagaya, *Physical Review E*, 2020, **101**, 022702.

H. Orihara, Y. Harada, F. Kobayashi, Y. Sasaki, S. Fujii, Y. Satou, Y. Goto and T. Nagaya, *Physical Review E*, 2019, **99**, 012701.

E. W. Burkholder and J. F. Brady, *Soft Matter*, 2020, **16**, 1034–1046.

H. Seyforth, M. Gomez, W. B. Rogers, J. L. Ross and W. W. Ahmed, *Physical Review Research*, 2022, **4**, 023043.

C. Wang and H. Jiang, *Soft Matter*, 2020, **16**, 4422–4430.